Time-Frequency Localization Measures for Packets of Orthogonally Multiplexed Signals

Christopher Boyd, Renaud-Alexandre Pitaval, Olav Tirkkonen and Risto Wichman

***Abstract*—We consider measures of time-frequency localization (TFL) for stochastic signals. The approach is complementary to the use of TFL in prototype filter design; here, TFL is instead applied to multiplexed waveform packets, with the objective to evaluate multi-user interference in a multiple access scenario rather than combat channel dispersion. We show that a generalization of the Heisenberg parameter to N-dimensional stochastic signals directly characterizes the localization of the inter-user interference in the time-frequency phase space. A tight bound is provided that shows the fundamental trade-off between the TFL of a packet and orthogonality among the multiplexed waveforms inside the packet. Hermite-Gauss waveforms are optimally localized with regard to this measure. We also derive expressions for the TFL of a Gabor system consisting of N_t time- and N_f frequency-shifts of a prototype, on conventional and staggered lattices. In the limit of large N, the particular properties of the prototype yield diminishing returns to the overall localization. Lastly, we compare the performance of waveforms in a connectionless and asynchronous random access scenario. At lower access intensities, where the out-of-band emissions are the significant limiting factor, the outage probability for smaller access packets is shown to vary significantly between modulations. This variability diminishes when N is increased, consistent with the presented theory.**

***Index Terms*—Time-frequency localization, Heisenberg parameter, stochastic signals, orthogonal multiplexing, Hermite-Gauss functions, asynchronous random access.**

I. Introduction

A major challenge in the design of waveforms for communications is to maintain orthogonality, to facilitate the optimal recovery of signals over noisy channels while trading off time-frequency localization (TFL) and waveform density. Strictly localized waveforms minimize spectral leakage and provide robustness in dispersive channels, while a higher waveform density generally corresponds to a better spectral efficiency [1].

In a communication scenario where there are simultaneous radio transmissions conducted on adjacent time slots and/or frequency carriers, it is vital to control and mitigate the inevitable leakage of power, and consequential interference, between the transmissions. This can be aided by the use of well-designed prototype waveforms, strictly contained in the time and frequency domains as to limit their mutual interference properties with their translated neighbors. Conventionally, measures of this interference include the adjacent channel leakage ratio (ACLR), adjacent channel selectivity (ACS), and inter-symbol interference (ISI).

The Heisenberg parameter is a measure of the time-frequency localization of a given waveform, related to Heisenberg's well-known uncertainty principle from quantum mechanics [2], [3]. It states that a function and its Fourier transform cannot be simultaneously well-localized, a limitation which follows from Fourier analysis. The Heisenberg parameter is adopted in the literature as a convenient catch-all measure describing the overall interference leakage properties of waveforms [4]–[7]. Discussions involving the Heisenberg parameter in the literature consider the TFL of a single waveform, a prototype filter, upon which Gabor systems are built [4]. The idea is to produce multicarrier waveforms that are robust against channel dispersion.

In this paper, we consider the overall localization of a transmission packet consisting of a number of orthogonal waveforms, expanding upon our work in [8]. This is a complementary perspective to considering the TFL of a prototype filter. Instead of minimizing intra-user interference in time and frequency selective channels, we are interested in the interference caused between uncoordinated transmissions from multiple users in frequency flat channels. Such analysis is motivated by the paradigm shift in wireless communication technologies towards relaxed synchronization constraints and uncoordinated transmission [9], [10]. While the impact of the prototype filter's TFL on the orthogonality and power leakage inside a single user's transmission will remain important to mitigate channel dispersion, of equal concern in an asynchronous system will be the external interference properties of the transmissions. Intuitively, by imposing orthogonality on the component waveforms one limits the achievable TFL of the overall transmitted packet. For example, out-of-band (OOB) power reduction methods for orthogonal frequency-division multiplexing (OFDM), such as filtering or windowing, typically rely on increasing the time-dispersion and/or sacrificing orthogonality between the component waveforms.

The main contributions of this paper are as follows:

- We generalize the Heisenberg parameter applied to a stochastic signal constructed from a family of N waveforms modulated by statistically independent symbols, and show that this measure describes the overall localization characteristics of the signal from

Christopher Boyd and Olav Tirkkonen are with the Department of Communications and Networking, Aalto University, Finland (email: {christopher.boyd, olav.tirkkonen}@aalto.fi). Renaud-Alexandre Pitaval was with the Department of Communications and Networking, Aalto University, Finland, he is now with Huawei Technologies Sweden (email: renaud-alexandre.pitaval@alumni.aalto.fi). Risto Wichman is with the Department of Signal Processing and Acoustics, Aalto University, Finland (email: risto.wichman@aalto.fi). Part of this work was presented at the 2015 IEEE International Workshop on Signal Processing Advances in Wireless Communications.

the perspective of interference victims. We stress that from the perspective of the intended receiver of such a transmission, the performance of component waveforms inside the signal in dispersive channels is not fully captured by the generalized Heisenberg parameter (GHP).

- For a stochastic signal consisting of orthogonal waveforms spanning an N-dimensional subspace in the Hilbert space of square integrable functions, the presented Heisenberg-type analysis leads to a TFL bound inversely proportional to N. It means that for designing packets of orthogonally multiplexed signals there is a fundamental trade-off between TF-localization of the packet and orthogonality among the component waveforms.
- In terms of the GHP measure, an optimal basis for constructing N-dimensional stochastic waveforms consists of the N Hermite-Gauss functions based on polynomials with the lowest degree. In [6], [11]–[13], linear combinations of Hermite-Gauss functions were used for the design of well-localized prototype filters for Gabor systems, while in [14], Hermite-Gauss functions were used in a multipulse multicarrier system. Due to optimal GHP, this family is a good orthogonal basis for designing multiplexed stochastic signals. Here, stemming from the optimal localization of this family of functions, we identify it as a good orthogonal basis for designing multiplexed stochastic signals not limited to Gabor systems.
- Additionally, we derive the time-frequency localization of a Gabor system consisting of some N_t translations and N_f modulations of a prototype waveform, as well as large-dimensional limits on the TFL for Gabor systems constructed using common prototypes. The analysis reveals that the TFL of Gabor systems is asymptotically tending to the same constant as N_t and N_f become large, irrespective of the prototype.
- We address the localization properties of cross-ambiguity functions and the related interference potential between transmitted multidimensional packets, and show a direct connection between the localization of interference and the GHP of the packets.
- Finally, we examine the merit of the presented generalized TFL measures, and explore the relationship between a waveform packet's localization and its interference potential in time and frequency, with a case study involving connectionless and asynchronous random access, a 5G use case [9]. We compare the random access channel (RACH) performance for various modulation formats against what is predicted by the GHP.

The paper is structured as follows. Section II introduces the system model and the notion of stochastic signals as Gabor systems. Section III follows with a short overview of relevant topics in the time-frequency analysis of individual waveforms. Section IV presents novel TFL measures for N-dimensional stochastic signals constructed from families of orthogonal waveforms, and relevant bounds and limits. The respective localization of common modulation schemes are compared with regard to these measures. Sections V explores the relationship between the GHP and a stochastic signal's interference potential, and Section VI includes a case study with asynchronous random access illustrating the relevance of the presented localization measures. Finally, Section VII offers conclusions.

II. System Model

In this work, we are concerned with waveforms and their properties in multiple access scenarios, where independent transmissions of information-carrying stochastic signals may suffer from mutual interference. Here we shall consider families of waveforms based on both time-frequency Gabor lattices, and more general families of orthogonal waveforms.

A. Stochastic Signals

Consider a point-to-point multi-carrier communication scenario. The transmitted signal is typically a stochastic signal consisting of a number of orthogonal component waveforms modulated by random constellation symbols

$$x\left(t\right)=\sum_{k=0}^{N-1}s_{k}\varphi_{k}(t), \tag{1}$$

where $\{\varphi_k\}$ is a set of N waveforms in $L^2\left(\mathbb{R}\right)$ and $\{s_k\}$ the corresponding set of symbols in $\mathbb{C}$.

B. Orthogonality and the Ambiguity Function

Upon reception over an ideal channel, all symbols s_k will be separable if an only if the orthogonality condition is met, i.e.

$$\langle\varphi_{k},\varphi_{l}\rangle=\int_{\mathbb{R}}\varphi_{k}(t)\varphi_{l}^{*}(t)dt=\delta_{k}\delta_{l}, \tag{2}$$

where $\delta_{k,l}$ is the Kronecker delta.

The cross-ambiguity function is a two-dimensional correlation function in phase space (or time-frequency plane), which for square-integrable functions $\varphi_k(t)$ and $\varphi_l(t)$ is defined as

$$A_{kl}(\tau,f)=\int_{\mathbb{R}}\varphi_{k}(t)\varphi_{l}^{*}(t+\tau)e^{-j2\pi ft}dt. \tag{3}$$

C. Gabor Systems

In conventional multi-carrier communication systems, the component waveforms $\{\varphi_k\}$ of transmitted signal $x(t)$ are modulations and translations in a two-dimensional phase space [15] of a single prototype filter $\varphi(t)\in L^2(\mathbb{R})$, also known as a Gabor atom. The resulting transmission functions are given by

$$\varphi_{n,m}\left(t\right)=\varphi\left(t-nT\right)e^{j2\pi mFt}, \tag{4}$$

where $n=0,...,N_t-1$ is the time index, T is the symbol duration, and $m=0,...,N_f-1$ and F are the subcarrier index and spacing, respectively. The family of $N=N_t\times N_f$ square integrable functions $\{\varphi_{n,m}(t)\}$ is a *Gabor system*, where the atom is centered around the origin $(0,0)$, and each $\varphi_{n,m}(t)$

around its corresponding coordinate (n, m). The lattice density is given by

$$\rho = (TF)^{-1}. \tag{5}$$

Ideally, the waveforms $\{\varphi_{n,m}(t)\}$ would be mutually orthogonal and well-localized, and spectral efficiency would be maximized by selecting T and F such that the lattice density $\rho = 1$. However, the Balian-Low theorem prohibits these conditions from being satisfied simultaneously, with the consequence that spectral efficiency must be sacrificed $(\rho < 1)$ in order to mitigate interference caused by dispersion [5], [16]. Lattices need not be rectangular as in (4) — hexagonal lattices have been shown to be superior in some cases [5], [13].

The Gabor system $\{\varphi_{n,m}(t)\}_{(n,m)\in\mathbb{Z}^2}$ is orthogonal if the ambiguity function satisfies

$$A(nT, mF) = \begin{cases} 1, & n, m = 0 \\ 0, & \text{otherwise.} \end{cases}. \tag{6}$$

In this paper, three types of Gabor systems will be considered, collectively referred to as *rectangular* Gabor systems. Both *staggered* and non-staggered lattices will be considered.

1) OFDM: In conventional OFDM, the prototype filter $\varphi(t)$ is a rectangular pulse of width T. This has the consequence that OFDM waveforms are poorly localized in frequency [17], [18]. Windowing functions can be used to mitigate OOB emissions [4], [19]. Here, we define windowed OFDM by a ramp-up/down duration T_{ramp}, which is the total time in excess of T that the prototype is spread by the windowing function.

2) FBMC: FBMC employs advanced prototype filters which are well-localized in frequency and greatly reduce OOB emissions [20]–[23]. An offset quadrature amplitude-modulated (OQAM) scheme is typically used, where the real and imaginary parts of each data symbol are transmitted on alternating component waveforms, resulting in a data rate being reduced by a factor of two when compared with OFDM [24]. To compensate for this, the real and imaginary parts are inserted at half symbol intervals $T/2$, forming a staggered lattice. This enables FBMC to circumvent the Balian-Low theorem and utilize well-localized prototypes filters such as the isotropic orthogonal transform algorithm (IOTA) filter [17], while maintaining spectral efficiency and achieving an effective density of $\rho = 1$. Note that all discussion and results regarding FBMC to follow will concern the IOTA prototype.

3) Single Carrier RRC: Root-raised-cosine (RRC) is a zero-ISI pulse shape which has the advantage of an adjustable "roll-off factor" α that trades off various design considerations.

III. Time-Frequency Analysis of a Single Waveform

We are interested in the time-frequency resource usage of multidimensional stochastic signals of the form (1). The time-frequency localization properties of single waveforms are well understood in the literature. These properties are important when constructing Gabor systems, and optimizing the performance of multicarrier waveforms in dispersive channels.

The time-frequency localization of a function is inversely related to the product of its inherent dispersion in both dimensions. The limitations on confining the dispersion simultaneously in both time and frequency follow directly from the uncertainly principle [25], [26]. TFL may be measured by the Heisenberg parameter ξ, which is bounded by the uncertainty principle. For a square-integrable function $\varphi(t) \in L_2(\mathbb{R})$, the parameter is given by [17]

$$\xi \triangleq \frac{\|\varphi\|_2^2}{4\pi\sigma_t(\varphi)\sigma_f(\hat{\varphi})} \leq 1, \tag{7}$$

where

$$\sigma_t(\varphi) \triangleq \left[\int_{\mathbb{R}} (t-\bar{t})^2 |\varphi(t)|^2 dt\right]^{\frac{1}{2}}, \tag{8}$$

is the standard deviation of the signal energy around the mean time

$$\bar{t}(\varphi) \triangleq \int_{\mathbb{R}} t|\varphi(t)|^2 dt, \tag{9}$$

characterizing the time dispersion of the signal. Similarly, $\sigma_f(\hat{\varphi})$ and $\bar{f}(\hat{\varphi})$ are the standard deviation and mean in the frequency domain, where $\hat{\varphi}$ denotes the Fourier transform of φ. Here $\|\cdot\|_2$ is the L^2-norm. Note that if φ is centered at $(0, 0)$, then $\bar{t}, \bar{f} = 0$. A filter that is well-localized has ξ close to 1, and equality holds in (7) if and only if $\varphi(t)$ is a Gaussian pulse [5], [27], [28].

Table I reports the TFL of common prototypes. OFDM has density $\rho = 1$ and $\xi = 0$ due to the unbounded variance in frequency, while windowed OFDM (wOFDM) and RRC have non-zero TFL and density $\rho < 1$.

Table I
TFL of Known Prototypes

	σ_t	σ_f	ξ
OFDM ($T = 1$)	0.289	∞	0
wOFDM ($T = 1, T_{\text{ramp}} = 1/64$)	0.292	1.775	0.154
wOFDM ($T = 1, T_{\text{ramp}} = 1/2$)	0.403	0.275	0.717
FBMC (IOTA, $T = 1$)	0.286	0.286	0.975
RRC ($T = 1, \alpha = 0.1$)	0.791	0.289	0.348
RRC ($T = 1, \alpha = 0.5$)	0.354	0.309	0.729
Gaussian	0.282	0.282	1

IV. TFL Measures for Stochastic Signals

For a signal constructed as in (1), a stochastic generalization of the Heisenberg parameter can be derived. This follows from investigating the TFL of well-localized families of waveforms.

A. Generalized Heisenberg Parameter

Recall the transmit signal of N complex symbols $\{s_k\}$ in (1), and consider the case where $\varphi_k(t) \in L^2(\mathbb{R})$ are unit-norm waveforms which are not necessarily orthogonal. With linear modulation, this is a sum of N random signals. The randomness is in the symbols, here assumed to be independent

and identically distributed (i.i.d) with zero mean and variance $E[|s_k|^2] = 1$. The time-frequency localization of this signal is itself random, and changes depending on the possible realizations of the signal. Typically, frequency containment of communication signals, e.g. frequency spectrum mask requirements, are defined through the power spectral density (PSD) of the signal, which can be obtained from the auto-correlation function. Accordingly, we will define a generalized Heisenberg parameter based on the average properties of the signal.

The average[1] time mean of stochastic signal x is given by

$$\tilde{\mu}(x) \triangleq \mathrm{E}[\bar{t}(x)] = \sum_k \int_{\mathbb{R}} t|\varphi_k(t)|^2 dt = \sum_k \bar{t}(\varphi_k), \quad (10)$$

and similarly by $\tilde{\mu}(\hat{x})$ in frequency. The average variance expressing the time dispersion of x is

$$\tilde{\sigma}_t^2(x) \triangleq \mathrm{E}[\sigma_t^2(x)] = \sum_k \int_{\mathbb{R}} (t - \tilde{\mu}(x))^2 |\varphi_k(t)|^2 dt, \quad (11)$$

and $\tilde{\sigma}_f^2(\hat{x})$ in frequency. The average power is simply the sum of the component waveform powers $\mathrm{E}[\|x\|^2] = \sum_k \|\varphi_k\|^2$. The GHP of this stochastic signal is

$$\tilde{\xi} \triangleq \frac{\mathrm{E}[\|x\|^2]}{4\pi \tilde{\sigma}_t(x) \tilde{\sigma}_f(\hat{x})} \leq 1. \quad (12)$$

The upper bound in (12) is a by-product of the uncertainty principle (7) which guarantees that, for any signal x, we have $\|x\|^2 \leq 4\pi \sigma_t(x) \sigma_f(\hat{x})$. Averaging on both sides and applying the Cauchy-Schwarz inequality, we get $\mathrm{E}\left[\|x\|^2\right] \leq 4\pi \sqrt{\mathrm{E}\left[\sigma_t^2(x)\right] \mathrm{E}\left[\sigma_f^2(\hat{x})\right]} = 4\pi \tilde{\sigma}_t(x) \tilde{\sigma}_f(\hat{x})$.

The time-frequency localization $\tilde{\xi}$ of the stochastic signal matches the conventional Heisenberg parameter ξ of a sample realization with a single waveform.

B. Bound on the GHP for Orthogonally Multiplexed Stochastic Signals

Imposing an orthogonality constraint on the component waveforms modifies the maximum achievable statistical TFL for N-dimensional waveforms.

Proposition 1. *Consider a stochastic signal $x = \sum_k s_k \varphi_k$, where $\{\varphi_k\}$ is a family of N orthonormal waveforms, and $\{s_k\}$ are i.i.d. zero mean random numbers with $E[|s_k|^2] = 1$. Maintaining orthogonality among the N multiplexing waveforms reduces the best achievable time-frequency localization of the signal by N as*

$$\tilde{\xi} = \frac{\mathrm{E}[\|x\|^2]}{4\pi \tilde{\sigma}_t(x) \tilde{\sigma}_f(\hat{x})} \leq \frac{1}{N}, \quad (13)$$

where the time and frequency dispersions $\tilde{\sigma}_t$ and $\tilde{\sigma}_f$ of x are defined in (11)*.*

[1]Because data symbols are random, the time/frequency mean and time/frequency variance of the signal as computed in (8) and (9) are random. It follows that in Eq. (10) and (11) two averagings are taken into account: a statistical expectation over symbol randomness in s_k, and a time/frequency integration over the signal as in (8) and (9). Note that normalization of time/frequency averaging will be explicitly handled in (12).

This bound follows from a generalization of the Rayleigh quotient theorem to the Hilbert space, and the Mean-Dispersion Principle [29]. See Appendix A for details. It can also be seen as a special case of the problem considered in [30] where the correlation operator of the generic signal considered therein has only N non-zero all-equal eigenvalues.

By normalizing the GHP in (12) by the upper bound in (13), we define the following TFL measure for N-dimensional stochastic signals

$$\Xi \triangleq N\tilde{\xi} \leq 1. \quad (14)$$

Note that here we use Fourier analysis and a related computation of the L^2 variance to measure the number of time-frequency degrees of freedom required by a transmission. The above measure captures the intuitive notion of the time-frequency resources required by one transmitter transmitting N orthogonal waveforms, and the essential frequency occupied by such a transmission from the perspective of another transmitter. For $N = 1$, the conventional Heisenberg parameter effectively considers each transmission of a symbol as coming from a different transmitter. Due to the uncertainty relation, any waveform is unavoidably spread in time and/or frequency. For a signal consisting of multiple component waveforms, these components are partially spread into the domains of their neighbors and, as long as they remain mutually orthogonal, the resulting dispersion of the signal is only potentially harmful to adjacent transmissions. The above GHP captures the degree of time-frequency dispersion for a family of orthogonal waveforms, outside of the fundamental time-frequency resources occupied by the orthogonal transmissions. Fundamentally, this measure shows in which sense N orthogonal waveforms occupy at least N units of time×frequency.

C. Optimally Localized Basis with Respect to the GHP

The family of N orthogonal waveforms that is optimally localized and meets $\Xi = 1$ can be found. The Hermite-Gauss (HG) functions are the product of the Gaussian pulse and the orthogonal Hermite polynomials, and are defined as

$$\varphi_k^{\mathrm{HG}}(t) = \frac{2^{1/4}}{\sqrt{k! 2^k}} \left(\frac{-1}{\sqrt{2\pi}}\right)^k e^{\pi t^2} \left(\frac{d}{dt}\right)^k e^{-2\pi t^2}, \quad (15)$$

for all $k \in \mathbb{Z}^+$. The HG functions are mutually orthogonal [30], [31], and are eigenfunctions of the Fourier transform and $\hat{\varphi_k} = j^{-k}\varphi_k$, such that, for some $f \in L_2(\mathbb{R})$, $\langle f, \varphi_k \rangle = \langle \hat{f}, \hat{\varphi_k} \rangle = j^k \langle \hat{f}, \varphi_k \rangle$.

As it is the case for the IOTA and RRC prototype filters, the support of the HG functions is theoretically infinite. Nevertheless, these functions are mostly characterized on a compact support of few time units with nearly-zero infinite tails. For practical purpose, the tails can thus be truncated or windowed without noticeable impacts on their properties as it is typically done for implementation of common FBMC prototypes [4].

For the normalized Hermite-Gauss functions, the cross-ambiguity function is [6]

$$A_{kl}^{\mathrm{HG}}(\tau,f) = \frac{l!}{\sqrt{k!}\sqrt{l!}}(\sqrt{\pi}(\tau+jf))^{k-l}e^{-\frac{\pi}{2}(\tau^2-2j\tau f+f^2)} L_l^{(k-l)}(\pi(\tau^2+f^2)), \quad (16)$$

where $L_n^{\alpha}(m)$ are the Laguerre polynomials.

The generalized Heisenberg parameter (13) reaches its upper bound if the N orthonormal basis functions in $L^2(\mathbb{R})$ are the Hermite-Gauss pulses $\{\varphi_k^{\mathrm{HG}}\}_{k=0}^{N-1}$. The kth Hermite-Gauss function has zero mean and variance in time and frequency equal to $\sigma_t^2(\varphi_k) = \sigma_f^2(\hat{\varphi}_k) = \frac{2k+1}{4\pi}$. Therefore, the generalized Heisenberg parameter for a N-dimensional signal whose basis in $L^2(\mathbb{R})$ is the Hermite basis is $\tilde{\xi}_{\mathrm{HG}} = \frac{1}{N}$, and it follows that $\Xi_{\mathrm{HG}} = 1$.

We remark that while the HG functions $\{\varphi_k^{\mathrm{HG}}\}$ form a family of maximizers of the GHP, only φ_0^{HG} is individually a maximizer of the standard Heisenberg parameter. For example, we have $\xi = 1/3$ and $\xi = 1/5$ for φ_1^{HG} and φ_2^{HG}, respectively.

D. Time-Frequency Localization of Gabor Systems

The TFL measure and the associated bound in (14) are valid for all N-dimensional stochastic signals. In the case where signal x is a Gabor system, whose lattice consists of some N_t time translations and N_f frequency modulations of the atom, we may derive an additional expression for the TFL with its limit specific to Gabor systems.

Proposition 2. *If the stochastic multidimensional signal x is a rectangular Gabor system with prototype filter φ on a $N_t \times N_f = N$ lattice, the squared generalized Heisenberg parameter (13) is*

$$\tilde{\xi}_{\mathrm{Gabor}}^2 = \frac{1}{16\pi^2(\sigma_t^2(\varphi)+\frac{T^2}{12}(N_t^2-a))(\sigma_f^2(\varphi)+\frac{F^2}{12}(N_f^2-1))}, \quad (17)$$

where the prototype has length T and spacing F, and $a = 1$ for a conventional lattice, while $a = 1/4$ for a staggered lattice such as in OQAM.

Proof: The dispersion of stochastic signal x in time $\tilde{\sigma}_t^2(x)$ amounts to N_f times the contribution of N_t component waveforms occupying the same frequency resources. Since these waveforms are all the prototype φ, $\tilde{\sigma}_t^2(x)$ can be readily found in terms of $\sigma_t^2(\varphi)$ and the means of N_t time components. The frequency dispersion $\tilde{\sigma}_f^2(x)$ can be found by analogy, and (17) follows directly. See Appendix B for details. ∎

By normalizing (17) in Prop. 2, and taking the limit as the number of component waveforms in time and frequency tend to infinity, we observe the following.

Corollary 1. *The TFL according to (14) of any N_tN_f-dimensional Gabor system of density ρ is tending to the same constant as $N_t, N_f \to \infty$,*

$$\lim_{N_t,N_f\to\infty}(N_tN_f)^2\tilde{\xi}_{\mathrm{Gabor}}^2 = 9\rho^2/\pi^2. \quad (18)$$

This reveals the surprising result that the properties of the prototype filter have *no impact* of the time-frequency localization of a N-dimensional stochastic signal when the number of component waveforms is sufficiently large. As the number of component waveforms increases, their collective shape becomes increasingly rectangular in time and frequency. The limit corresponds to the TFL of a single non-realizable waveform which is perfectly rectangular in both domains. Such a waveform would have a variance in time and frequency equal to $\sigma_t^2 = \frac{T^2}{12}$ and $\sigma_f^2 = \frac{F^2}{12}$, respectively. For a hypothetical Gabor system constructed using N of these pulses, with density $\rho = 1$, the normalized generalized Heisenberg parameter (14) is independent of N, and one has $\Xi_{\mathrm{2D-rect}}^2 = N^2\tilde{\xi}_{\mathrm{Gabor}}^2 = 9/\pi^2$.

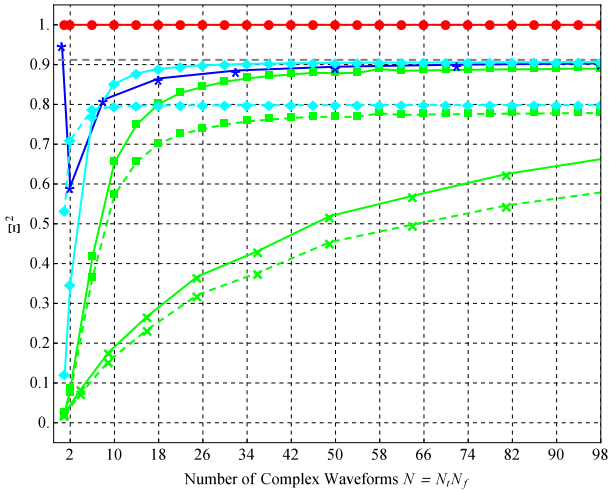

Figure 1. TFL of Hermite-Gauss, windowed OFDM ($T_{\mathrm{ramp}} = T/64$), RRC (with roll-off factor α), and FBMC (IOTA), as measured by the GHP.

Remark 1. *For a single-symbol multicarrier transmission with $N_t = 1$ and $N = N_f$ and finite variance $\sigma_f^2(\phi)$, the asymptotic of the GHP is given by*

$$\lim_{N_f\to\infty} N_f^2\tilde{\xi}_{\mathrm{Gabor}}^2 = \frac{3}{4\pi^2F^2\sigma_t^2(\varphi)}. \quad (19)$$

For windowed OFDM with $F = 1$ and $T_{\mathrm{ramp}} = T/64$ this is approximately $\Xi^2 \to 0.893$ without cyclic prefix and $\Xi^2 \to 0.781$ with 7% CP, for example. Only the time dispersion $\sigma_t^2(\varphi)$ impacts this asymptotic TFL.

Remark 2. *For single-carrier transmission with $N_f = 1$ and $N = N_t$ and finite variance $\sigma_t^2(\phi)$, the asymptotic of the GHP is given by*

$$\lim_{N_t\to\infty} N_t^2\tilde{\xi}_{\mathrm{Gabor}}^2 = \frac{3}{4\pi^2T^2\sigma_f^2(\varphi)}. \quad (20)$$

For single carrier RRC with $T = 1$ this is approximately $\Xi^2 \to 0.907$ for roll-off $\alpha = 0.1$ and $\Xi^2 \to 0.798$ for $\alpha = 0.5$, for example. Only the frequency dispersion $\sigma_f^2(\varphi)$ impacts this asymptotic TFL.

The values computed in remarks 1 and 2 equal the limit of the TFL for Gabor systems of these prototypes.

E. Numerical Comparisons

Figure 1 compares the TFL of HG, windowed OFDM, single carrier RRC and FBMC-OQAM stochastic signals as a function of the number of complex baseband waveforms N. The number of waveforms used varies between 1 and 98, and a complex information symbol is transmitted on each waveform. The generalized TFL measure can be seen to capture well the predicted behavior as the number of complex waveforms increases.

1) OFDM: In the case of OFDM, we employ a simple ramp-up, ramp-down window with $T_{\text{ramp}} = T/64$, and compute the TFL both with and without a CP. The CP overhead is assumed to be 7%, as in LTE, and the ramp-up/down is taken after the addition of the CP. Figure 1 describes two cases for OFDM, one where N is simply the number of subcarriers, i.e. $N = N_f$, and one where the lattice is square, i.e. $N_t = N_f = \sqrt{N}$. For small N, the cost of increased time dispersion from the windowing is compensated for by gains in frequency dispersion, though much less rapidly in the latter case. As more orthogonal waveforms are considered, frequency localization improves automatically and the TFL in both cases approaches the limit in (18), though again much less rapidly for the square lattice. We observe how the CP induces an asymptotically constant cost as $N \to \infty$ due to the increased time dispersion. The limits of the TFL in each case are exactly as predicted in (18) and (19).

2) FBMC: FBMC: In FBMC-OQAM, the prototype filter represents half a complex waveform, corresponding to the data point in Figure 1 at $N = 0.5$. This point does not by itself represent a Gabor system and unlike others is not normalized by the number of complex dimensions, i.e. it does not follow the definition of Ξ. While the TFL of the IOTA filter is unmatched, as a prototype for a small Gabor system (e.g. $N = 2$) it does suffer from increased dispersion in both time and frequency, arising from the OQAM staggered lattice approach. At $N = 2$ there are 4 real-valued and half-shifted component waveforms, which is not comparatively well-localized inside of 2 T-F resources. Despite this, FBMC with IOTA remains superior to windowed OFDM for all N, and converges to the TFL limit for Gabor systems much more rapidly. Note that the lattice is selected here to be as square as possible, such that $N_t = N_f = \sqrt{N}$.

3) RRC: Figure 1 also includes the TFL for single-carrier RRC as a function of the number of complex component waveforms. Root raised cosine waveforms are ideally localized in frequency, and orthogonal in time shifts of a symbol period. The roll-off factor α trades off dispersion in frequency against dispersion in time. In the plot, N time-shifted RRC pulses are considered, such that $N = N_t$. It can be observed how a larger roll-off produces the best localized Gabor system for $1 < N < 6$, while a much smaller roll-off α is superior for $N > 6$. The larger roll-off introduces an asymptotically constant cost to the TFL due to the increased time dispersion, as did the CP for OFDM, while a smaller α is poorly localized for small N but rapidly approaches the limit for Gabor systems. Single carrier RRC with a 10% roll-off outperforms all other Gabor systems considered with respect to the GHP. The limits of the TFL as N grows are as predicted in (20) for both roll-offs shown.

V. Localization of Phase Space Interference

The generalized Heisenberg parameter is inversely proportional to a rectangular area where most of the packet's energy resides in phase space, i.e. $\tilde{\xi} \propto \mathcal{A}^{-1}$ where $\mathcal{A} = \tilde{\sigma}_t \times \tilde{\sigma}_f$. Indeed, Chebyshev's inequality ensures that at least a $\left(1 - \frac{1}{k^2}\right)$-portion of the packet's energy is located within $k\tilde{\sigma}_t$ time-resources from the mean time, and similarly $k\tilde{\sigma}_f$ frequency-resources from the mean frequency. When two packets collide, the interference is intuitively the result of the 'overlap' of the packets, which depends of the area occupied by each packet in phase space. Nevertheless, this interpretation is only intuitive as signals are not exactly two dimensional functions in phase space. Instead, the interference power is derived through ambiguity functions, which are then precisely 2D functions whose support can be characterized by such an area in phase space. This section makes such a connection explicit.

A. Phase Space Interference Potential Function

To understand the connection between the localization of the transmitted multidimensional packet (1) and the spreading of interference in phase space, we shall consider the localization characteristics of the interference in phase space. Consider detecting the symbols s_k of the multidimensional stochastic packet $x(t)$ of (1), when there is an interfering transmission of a packet with the same number of symbols and the same basis functions. The difference of the centers of the wanted signal and interfering packet in phase space is (τ, f). At this stage we assume unit channel gain per dimension.

When matched filters are applied to receive the nearly orthogonal components ϕ_k of $x(t)$, the expected interference power disturbing the reception of symbol s_k is

$$I(\tau, f) = \frac{1}{N} \sum_{k,l} |A_{kl}(\tau, f)|^2 \ , \tag{21}$$

for conventionally in-phase and quadrature moduated signals. The interference from waveform l when receiving waveform k is given by the square of the ambiguity function $A_{kl}(\tau, f)$. For simplicity, we assume that the power density of the desired multidimensional packet is centered at the origin, such that the time and frequency means (10) are $\tilde{\mu}(x) = \tilde{\mu}(\hat{x}) = 0$.

For Gabor systems, the interference potential function (21) simplifies, as there is just one prototype pulse, so that all cross-ambiguities can be expressed in terms of the prototype ambiguity $A(\tau_k, f_k)$, with phase space separations $(\tau + \tau_k, f + f_k)$. There is a difference lattice $\mathcal{D} \ni (\tau_k, f_k)$ encoding the differences between two Gabor transmission lattices. Different elements in the difference lattice may have different multiplicities. If considering lattice staggered FBMC, one has two distinct difference lattices, $\mathcal{D}_{\text{same}}$ for the lattice separations between the in-phase–in-phase and quadrature–quadrature branches of the wanted signal and interferer transmissions, and $\mathcal{D}_{\text{diff}}$

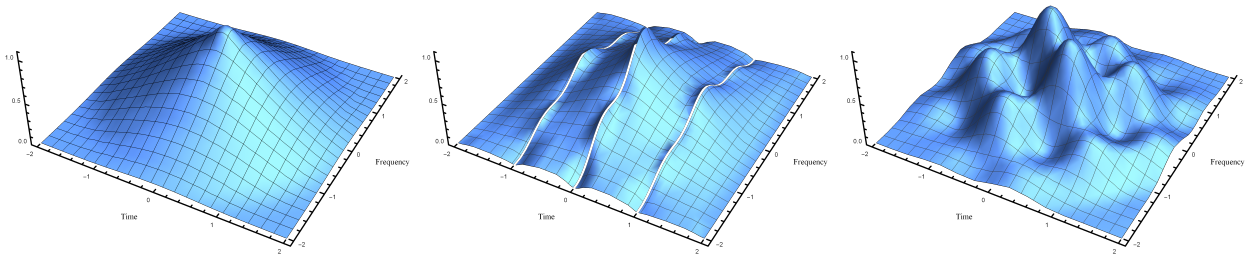

Figure 2. Interference potential functions for four-waveform packets for Hermite-Gauss (left), OFDM (middle), and FBMC-OQAM with IOTA prototype and channel phase $\Psi = \pi/4$ (right). The scale is in units of time-frequency.

for the lattice separations between in-phase–quadrature and quadrature–in-phase branches. Due to the separation of the in-phase and quadrature branches in phase space, the relative channel phase difference Ψ between the wanted signal and interfering signal will have an effect for lattice staggered FBMC. Thus, the interference will be characterized by $\left(\mathrm{Re}/\mathrm{Im}\left[e^{i\Psi}A(\tau_k, f_k)\right]\right)^2$, with (τ_k, f_k) in the appropriate difference set, and Re taken for $\mathcal{D}_{\mathrm{same}}$, while Im is taken for $\mathcal{D}_{\mathrm{diff}}$. The interference function then becomes a function $I(\tau, f, \Psi)$.

Figure 2 illustrates the interference function of packets of 4 waveforms in phase space, for HG, OFDM and FBMC-OQAM with the IOTA prototype pulse for a representative value of $\Psi = \pi/4$.

When there is a set of M interferers, with received power P_m and phase space difference τ_m, f_m, as compared to the signal of interest, the realized interference power experienced is given by the interference potential function evaluated at the locations of the interferers, as

$$I_{\mathrm{tot}} = \sum_{m=0}^{M-1} P_m \; I(\tau_m, f_m) \; . \tag{22}$$

The signal-to-interference ratio (SIR) for the wanted transmission is then $\gamma = P_0/I_{\mathrm{tot}}$.

B. Localization of Interference Potential Function

As can be seen in Figure 2, the phase space occupancy of the interference functions of different waveforms varies. It is of interest to understand the localization properties of these functions.

The L^2 localization characteristics of the interference potential function can be expressed in terms of the localization characteristics of the multidimensional stochastic wave packet. This leads directly to the following GHP for the interference potential function.

Proposition 3. *The GHP $\tilde{\xi}$ of N-dimensional packet x, defined in (12), can be expressed directly in terms of a GHP of the interference potential function as*

$$\tilde{\xi}^2 \;=\; \frac{N\;\mathrm{E}\left[I\right]}{4\pi^2\;\sigma_\tau^2(I)\;\sigma_f^2(I)} \;\leq\; \frac{1}{N^2}\;, \tag{23}$$

where the time-variance is defined by $\sigma_\tau^2(I) = \int(\tau - \mu_\tau(I))^2 I(\tau, f)\; d\tau df$ with time-mean $\mu_\tau(I) = \int \tau I(\tau, f)\; d\tau df$, and similarly for $\sigma_f^2(I)$ in frequency.

Proof: Consider the 2D variance of the squared cross-ambiguity function $|A_{kl}(\tau, f)|^2$. First, we observe that this function is normalized to one if the basis functions are normalized: using the definition (3) for $A_{kl}(\tau, f)$ we directly find

$$\begin{aligned}\int_{\mathbb{R}^2} |A_{kl}(\tau, f)|^2\, d\tau df &= \int |\varphi_k(t)|^2\, |\varphi_l(t+\tau)|^2\, d\tau dt \\ &= \|\varphi_k\|^2\, \|\varphi_l\|^2\,. \end{aligned} \tag{24}$$

The first equality follows from $\int e^{-2\pi i f(t-t')} df = \delta(t-t')$, and the second from a change of variables $t' = t + \tau$ with Jacobian determinant 1. It follows that the expectation of the interference potential over phase space is $\mathrm{E}\left[I\right] = \frac{1}{N}\mathrm{E}(\left[\|x\|^2\right])^2$.

For the raw time-variance (i.e. without subtracting the mean in the expectation) we find with the same steps as above

$$\begin{aligned}\sigma^2_{\tau,\mathrm{raw}}\left(A_{kl}\right) &\equiv \int \tau^2\, |A_{kl}(\tau, f)|^2\, d\tau df \\ &= \int |\varphi_k(t)|^2\, |\varphi_l(t')|^2\, (t-t')^2 dt' dt \\ &= \sigma_t^2(\varphi_k) + \sigma_t^2(\varphi_l) - 2\bar{t}\left(\varphi_k\right)\; \bar{t}\left(\varphi_l\right) \end{aligned} \tag{25}$$

Consider now the full interference potential. Following the same steps as in evaluating (24) we get for its time-mean $N\mu_\tau(I) = \sum_{k,l} \bar{t}(\varphi_k) + \bar{t}(\varphi_l) = 2\tilde{\mu}(x)$, which we can assumed to vanish without loss of generality. Using (25) we then get for the time-variance

$$\begin{aligned}\sigma_\tau^2\left(I\right) &\equiv \int \tau^2 I(\tau, f)\; d\tau df \\ &= \frac{1}{N}\sum_{k,l} \sigma_t^2(\varphi_k) + \sigma_t^2(\varphi_l) - 2\;\bar{t}\left(\varphi_k\right)\;\bar{t}\left(\varphi_l\right) \\ &= 2\sum_k \sigma_t^2(\varphi_k) - \frac{2}{N}\left(\sum_k \bar{t}\left(\varphi_k\right)\right)^2 \\ &\equiv 2\;\tilde{\sigma}_t^2(x)\;. \end{aligned} \tag{26}$$

Thus, the time-variance of the interference power function $I(\tau, f)$ is directly given by the time-variance (11) of the stochastic packet x.

For the frequency variance of the interference function, we correspondingly get $\sigma_f^2\,(I) = 2\,\tilde{\sigma}_f^2(\hat{x})$, which can be obtained by expressing the functions φ_k in the ambiguity function (3) by their Fourier transforms.

From Eq. (13) and (26), and the corresponding equation for the frequency variance, it follows that the GHP of x can be expressed directly in terms of a GHP of the interference potential function, as in (23). ∎

In the denominator of (23) in Prop. 3, we have the product $\mathcal{A}_{\mathrm{STD}} = \sigma_\tau(I)\ \sigma_f(I) = 2\tilde{\sigma}_t(x)\tilde{\sigma}_f(x)$ of standard deviations in time and frequency, which gives the area of the region in phase space where most of the interference potential of a waveform is concentrated. The L^2 localization of the interference potential is maximized when Hermite-Gauss basis functions are used.

C. Outage Measures for One Interferer

Now we consider precisely one interferer at phase space separation (τ, f), so that the interference is given directly by (21). We consider asynchronous transmissions, such that any arrival position (τ, f) of the interferer is possible. For simplicity, we assume that the received power of the wanted signal and the interferer are the same, and that noise is neglected. A guaranteed quality of service of the transmission can be characterized by a SIR threshold θ. This means that if $I(\tau, f) > 1/\theta$, the received SIR is below θ, and the transmission is expected to be in outage. For a given θ, and transmissions with a given set of basis functions, this translates to an *exclusion region in phase space*. If the packet is to be successfully received, no other transmissions can exist within this region.

For certain families of basis functions, the interference potential (21) may vanish at specific locations in phase space surrounded by small low-interference regions. For example, for OFDM, interference would vanish for fully synchronous transmissions in time and frequency, when frequency separation is a large enough integer multiple of subcarrier bandwidth. Here we assume that the interfering transmission is not consciously selected to have such time-frequency characteristics, and thus packet arrivals in such regions have low probability.

In Fig. 3, the areas of phase space exclusion regions are shown as a function of θ, for OFDM, FBMC-OQAM (with IOTA prototype) and Hermite-Gauss basis functions, and for packets of $N = 4$ and $N = 30$ orthogonal transmissions. These can be compared to the corresponding phase space areas defined by the products of the standard deviations $\mathcal{A}_{\mathrm{STD}}$ of the interference potentials. According to (23), these can be read directly from Fig. 1, and can be found in Table II. Note that the localization of the interference potential yields a precise L^2 measure of the number of time-frequency degrees of freedom required for a transmission. Furthermore, in Fig. 3 we see how the precise number of time-frequency degrees of freedom required for error free reception depends on the tolerance of the transmission to interference.

The vulnerability of OFDM to interference coming from large phase space separations is clearly visible, the area of

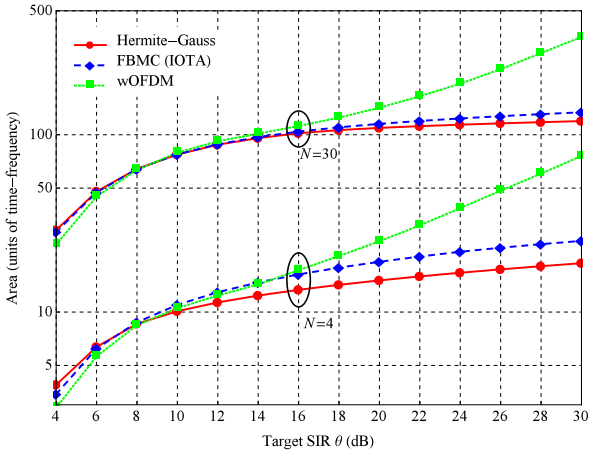

Figure 3. Areas of phase space exclusion regions for successful reception of transmissions requiring SIR threshold θ.

Table II
AREAS $\mathcal{A}_{\mathrm{STD}}$ IN PHASE SPACE, CORRESPONDING TO PRODUCTS OF STANDARD DEVIATIONS OF INTERFERENCE POTENTIAL FUNCTIONS

	$N = 4$	$N = 30$
wOFDM	5.69	41.3
FBMC-OQAM (IOTA)	1.54	26.8
Hermite-Gauss	1.30	26.7

the exclusion region grows increasingly with increasing SIR requirement. The ratio of the area of the exclusion regions reflects the ratio of the corresponding $\mathcal{A}_{\mathrm{STD}}$.

VI. Asynchronous Random Access Simulation

Above, we considered exclusion regions for packets with a single interferer. Here, we extend to a multiple access scenario. As discussed above, the localization characteristics of the interference potential becomes relevant in an asynchronous scenario. For Gabor systems, the interference potential function vanishes at certain isolated time-frequency points. In an asynchronous system, transmissions cannot be planned such that time-frequency separations fall to these points. The random access channel in the massive machine-type communications (mMTC) 5G use case is an environment where interference and collisions between transmissions are especially harmful, yet may be minimized by employing well-localized families of waveforms. Limiting the energy outside of a transmission's time and frequency resources will improve RACH outage probability and throughput. This is especially true in the case of asynchronous random access, which is expected to facilitate mMTC in 5G systems [10]. In a fully asynchronous RACH setting, the number of interferers is a random variable, the received signals are random, and the phase space separation between interferers in (22) are random as well.

A. Random Access Scenario

Consider a connectionless random access scenario, as in [9], where many users access a limited number of physical resources in a temporally and spectrally asynchronous and

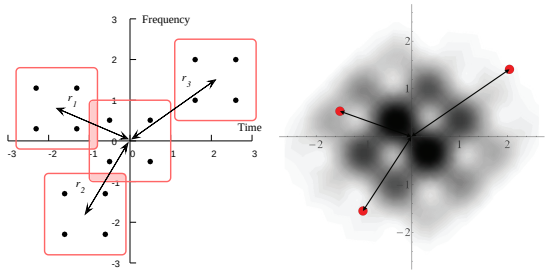

Figure 4. Four-waveform packet arrivals and collisions in phase space. Inter-arrival times and frequency offsets relative to a packet at origin. Left: Intuitive phase space occupation per packet and interference from collisions. Right: Reception of a packet at the origin, with interfering packets represented by points in an interference potential landscape. The grey shadow represents the level of interference at precise arrival locations in the surrounding phase space, here obtained by projecting the interference potential of FBMC in Figure 2 to the phase space. For each interfering packet, the level of interference it creates is the grey level at the precise red point location.

uncoordinated fashion, and transmit their payloads in a single burst with limited signaling. Dormant users awake and immediately transmit an access packet with maximum power. Each access packet contains N orthogonal complex component waveforms.

In such an uncoordinated asynchronous multiple access scheme, collisions resulting in interference will occur when time- and frequency-adjacent access packets overlap in phase space. Figure 4 illustrates how access packet arrivals occupy and collide in phase space. Also, the perspective of receiving one of the packets is shown, with interferers as points in an interference potential landscape.

We model a situation where there is band reserved for asynchronous random access, with bandwidth $>>$ $\sigma_f(\hat{x})$. Within this band, accessing transmissions choose the center frequency and center time uniformly at random. A conventional Poisson arrival process is considered for the time-domain arrivals. With the random choice of center frequency, the arrival process thus becomes 2D, with intensity λ per phase space unit area, i.e., per s Hz.

As the transmissions are performed without any measurements of network transmission, we assume that there is no power control and all users transmit with a fixed power. Accordingly, the received signal power of wanted transmissions and interfering transmissions at a receiver are random variables. We model these by frequency-flat Rayleigh fading, so that the received power of both the wanted signal, and the interferers are exponentially distributed, with mean 1. In addition, there is a relative channel phase Ψ_m between the wanted signal and interfering signal m. This channel phase will affect the interference of FBMC-OQAM, but not conventionally in-phase and quadrature modulated transmissions, such as OFDM or Hermite-Gauss waveforms. For simplicity, we neglect thermal noise and consider only multiple-access interference.

B. Random Access Outage Probability

If the sum interference power from all interfering transmissions in phase space, as compared to the received signal power of the wanted signal, is such that the received

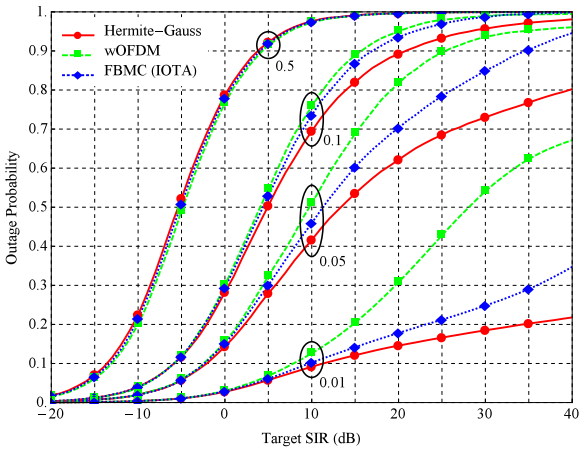

Figure 5. Outage probability in asynchronous random access for access intensities $\lambda = 0.01, \ldots, 0.5$, $N = 4$ waveforms.

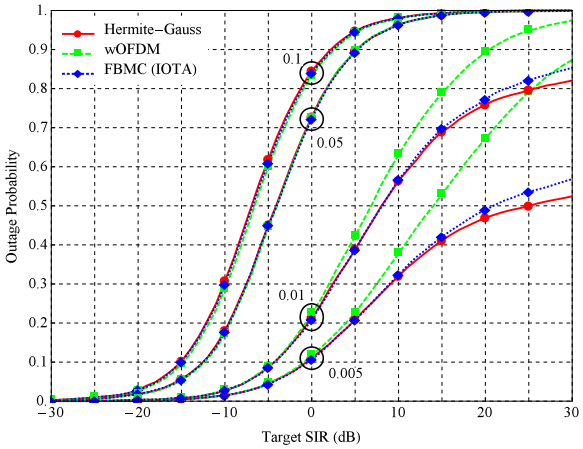

Figure 6. Outage probability in asynchronous random access for access intensities $\lambda = 0.005, \ldots, 0.1$, $N = 30$ waveforms.

SIR is less than the threshold θ, we declare an access attempt to be in outage. By simulation, we estimated the SIR experienced by an access packet over 100,000 time instances and realizations of the random channel, and the arrival process, and found the outage probabilities for windowed OFDM, FBMC-OQAM (IOTA) and Hermite-Gauss modulations. The outage probabilities for access packets of size $N = 4$ and $N = 30$ are presented in Figures 5 and 6, respectively.

Since packets of N waveforms occupy roughly N units of time-freqeuncy, the average interference increases with N for a fixed access intensity λ. We observe that for both $N = 4$ and $N = 30$, the modulations considered have comparable performance at higher intensities. With high access intensity, it is likely that the strongest interferers are located close to the center of a packet, in which case the specific localization characteristics of the packets become irrelevant.

At lower intensities, the GHP accurately predicts the performance. In this case, the localization characteristics of the interference potential become relevant, and thus the GHP of the stochastic packet. It can be observed that, as predicted by the analysis of the GHP, i) HG performs the best, while FBMC performs better than OFDM, but also ii) that these relative

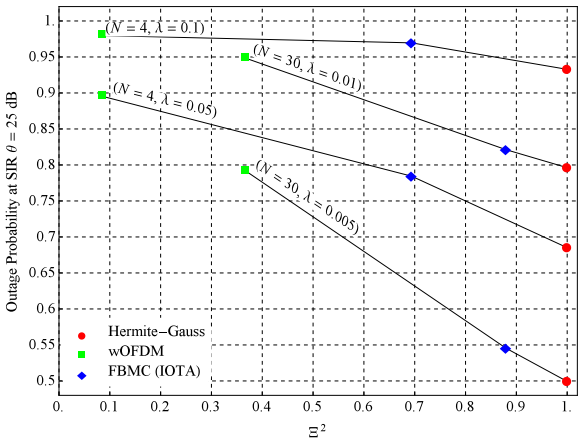

Figure 7. Outage probability at an SIR of 25 dB, as a function of the GHP of the packets for different intensities and packet sizes.

differences in performance are vanishing as N increases. These behaviors could not be inferred from the standard HP, as i) HG is made of several waveforms with different TFL, and ii) the standard Heisenberg parameter does not indicate any behavior as a function of N.

The dependency between the GHP of the packets and the outage probabilities at a fixed SIR in Fig. 5 and 6 is reported in Fig. 7. For a given intensity and packet size, it can be observed that the outage probability almost linearly decreases with the squared GHP, and thus appears to be correlated.

VII. Conclusions

In this paper, we have discussed time-frequency localization, a central concept in the design of transmission waveforms robust to dispersive channels. The TFL of a prototype waveform has heretofore been measured by the Heisenberg parameter, derived from the product of a signal's variance in both time and frequency domains and bound by the uncertainty principle. The measure describes a prototype's ability to, as a basis for a Gabor system, maintain orthogonality with its neighbors, and resist inter-symbol and inter-channel interference.

However, in asynchronous transmission scenarios, one is mostly concerned with the overall localization of a multi-dimensional signal constructed from a basis or family of orthogonal waveforms. We generalized the Heisenberg parameter to N-dimensional stochastic signals with its corresponding bound on the TFL, for signals constructed from orthogonal waveforms. The generalized measure captures a signal's dispersion outside of the time-frequency resources occupied by its mutually orthogonal component waveforms, and therefore quantifies its external interference potential. Furthermore, we have shown that the family of Hermite-Gauss waveforms forms the most well-localized basis for constructing such signals, with respect to the generalized Heisenberg parameter. In addition, we derived an expression for the TFL of a Gabor system constructed by time- and frequency-shifting a prototype waveform, a general limit for Gabor systems, as well as specific limits for a number of common prototypes.

A key result of the TFL analysis for N-dimensional stochastic signals as Gabor systems was that the specific properties of the prototype employed become irrelevant to the overall localization as the number of component waveforms increases. We observed that the TFL of windowed OFDM (without CP), FBMC-OQAM (with the IOTA prototype) and RRC (with infinitesimal roll-off) signals increases with the number of complex waveforms N, and converge towards the derived limit for Gabor systems. This limit was revealed to be the TFL of the unrealizable waveform that is rectangular in both time and frequency.

Lastly, we simulated a connectionless and asynchronous random-access scenario, and verified that the GHP predicts the relative performances of HG, OFDM and FBMC-OQAM modulated access bursts of various size. The variability in their performance was observed to diminish for larger access packets as predicted by the GHP. The relevance of the GHP for such communications scenario was supported by an analysis of the localization of the inter-user interference potential showing its direct characterization by the GHP of the packets.

Acknowledgment

This work was supported in part by the Academy of Finland (grant 284725), by EIT ICT Labs (HII:ACTIVE) and Nokia. OT and RW thank Kari Pajukoski and Esa Tiirola for discussions on the subject. We thank Prof. Matz for discussions, and for pointing out [14], [30] to us.

References

[1] G. Matz, H. Bölcskei, and F. Hlawatsch, "Time-Frequency Foundations of Communications: Concepts and Tools," *IEEE Signal Process. Mag.*, vol. 30, no. 6, pp. 87–96, Nov. 2013.

[2] P. Busch, T. Heinonen, and P. Lahti, "Heisenberg's Uncertainty Principle," *Phys. Rep.*, vol. 452, no. 6, pp. 155–176, Oct. 2007.

[3] G. B. Folland and A. Sitaram, "The Uncertainty Principle: A Mathematical Survey," *J. Fourier Anal. and Appl.*, vol. 3, no. 3, pp. 207–238, 1997.

[4] B. Farhang-Boroujeny, "OFDM versus Filter Bank Multicarrier," *IEEE Signal Process. Mag.*, vol. 28, no. 3, pp. 92–112, May 2011.

[5] T. Strohmer and S. Beaver, "Optimal OFDM Design for Time-Frequency Dispersive Channels," *IEEE Trans. Comm.*, vol. 51, no. 7, pp. 1111–1122, Jul. 2003.

[6] R. Haas and J.-C. Belfiore, "A Time-Frequency Well-Localized Pulse for Multiple Carrier Transmission," *Wireless Pers. Comm.*, vol. 5, no. 1, pp. 1–18, 1997.

[7] P. Siohan, C. Siclet, and N. Lacaille, "Analysis and Design of OFDM/OQAM Systems based on Filterbank Theory," *IEEE Trans. Sig. Process.*, vol. 50, no. 5, pp. 1170–1183, 2002.

[8] C. Boyd, R.-A. Pitaval, O. Tirkkonen, and R. Wichman, "On the Time-Frequency Localisation of 5G Candidate Waveforms," in *Proc. IEEE Int. Works. on Sig. Proc. Adv. in Wireless Comms.*, Jun. 2015, pp. 101–105.

[9] G. Wunder, P. Jung, M. Kasparick, T. Wild, and F. Schaich et. al., "5GNOW: Non-Orthogonal, Asynchronous Waveforms for Future Mobile Applications," *IEEE Comm. Mag.*, vol. 52, no. 2, pp. 97–105, Feb. 2014.

[10] G. Wunder, M. Kasparick, S. ten Brink, F. Schaich, and T. Wild et. al., "5GNOW: Challenging the LTE Design Paradigms of Orthogonality and Synchronicity," in *Proc. IEEE Veh. Tech. Conf.*, Dresden, Germany, Jun. 2013, pp. 1–5.

[11] T. Kurt, M. Siala, and A. Yonga coğlu, "Multi-Carrier Signal Shaping Employing Hermite Functions," in *Proc. IEEE Sig. Process. Conf.*, Antalya, Turkey, 2005, pp. 1–4.

[12] C. W. Korevaar, A. Kokkeler, P. de Boer, and G. Smit, "Closed-Form Expressions for Time-Frequency Operations Involving Hermite Functions," *IEEE Trans. Sig. Process.*, vol. 64, no. 6, pp. 1383–1390, Mar. 2016.

[13] ——, "Spectrum Efficient, Localized, Orthogonal Waveforms: Closing the Gap with the Balian-Low Theorem," *IEEE Trans. Comm.*, vol. 64, no. 5, pp. 2155 – 2165, Feb. 2016.

[14] M. Hartmann, G. Matz, and D. Schafhuber, "Wireless multicarrier communications via multipulse Gabor Riesz bases," *EURASIP J. Applied Sign. Proc.*, no. 23818, pp. 1–15, 2006.

[15] I. Daubechies, "Time-Frequency Localization Operators: A Geometric Phase Space Approach," *IEEE Trans. Inf. Theory*, vol. 34, no. 4, pp. 605–612, Jul. 1988.

[16] J. Benedetto, C. Heil, and D. Walnut, "Differentiation and the Balian-Low Theorem," *J. Fourier Anal. and Appl.*, vol. 1, no. 4, pp. 355–402, 1994.

[17] B. L. Floch, M. Alard, and C. Berrou, "Coded Orthogonal Frequency Division Multiplex," in *Proc. IEEE*, vol. 83, no. 6, 1995, pp. 982–996.

[18] H. Steendam and M. Moeneclaey, "Analysis and Optimization of the Performance of OFDM on Frequency-Selective Time-Selective Fading Channels," *IEEE Trans. Comm.*, vol. 47, no. 12, pp. 1811–1819, 1999.

[19] H. Bölcskei, P. Duhamel, and R. Hleiss, "Design of Pulse Shaping OFDM/OQAM Systems for High Data-rate Transmission over Wireless Channels," *IEEE Int. Conf. on Comm.*, vol. 1, pp. 559–564, 1999.

[20] M. Payaró, A. Pascual-Iserte, and M. Najar, "Performance Comparison between FBMC and OFDM in MIMO Systems under Channel Uncertainty," in *Proc. IEEE Eu. Wireless Conf.*, Apr. 2010, pp. 1023–1030.

[21] A. Şahin, I. Güvenç, and H. Arslan, "A Comparative Study of FBMC Prototype Filters in Doubly Dispersive Channels," in *Proc. IEEE Broadband Wireless Access Workshop*, Dec. 2012, pp. 197–203.

[22] M. Schellmann, Z. Zhao, H. Lin, P. Siohan, N. Rajathevaa, V. Luecken, and A. Ishaque, "FBMC-based Air Interface for 5G Mobile: Challenges and Proposed Solutions," in *Proc. Int. Conf. on Cog. Radio Oriented Wireless Net. Comm.*, Jun. 2014, pp. 102–107.

[23] P. Banelli, S. Buzzi, G. Colavolpe, A. Modenini, F. Rusek, and A. Ugolini, "Modulation Formats and Waveforms for 5G Networks: Who Will Be the Heir of OFDM?" *IEEE Signal Process. Mag.*, vol. 31, no. 6, pp. 80–93, Nov. 2014.

[24] F. Schaich, "Filterbank Based Multi Carrier Transmission (FBMC) - Evolving OFDM: FBMC in the context of WiMAX," in *Proc. IEEE Eu. Wireless Conf.*, Apr. 2010, pp. 1051–1058.

[25] L. Calvez and P. Vilbé, "On the Uncertainty Principle in Discrete Signals," *IEEE Trans. Circ. and Sys.*, vol. 39, no. 6, pp. 394–395, Jun. 1992.

[26] T. Przebinda, V. DeBrunner, and M. Ozaydin, "Using a New Uncertainty Measure to Determine Optimal Bases for Signal Representations," in *Proc. IEEE Int. Conf. Acoust., Speech, Signal Process.*, vol. 3, Phoenix, AZ, Mar. 1999, pp. 1365–1368.

[27] A. Şahin, I. Güvenç, and H. Arslan, "A Survey on Multicarrier Communications: Prototype Filters, Lattice Structures, and Implementation Aspects," *IEEE Comm. Surveys and Tutorials*, vol. 16, no. 3, pp. 1312 – 1338, Dec. 2014.

[28] A. Muzhikyan and G. Avanesyan, "Asymptotically Exact Localized Expansions for Signals in Time-Frequency Domain," *J. Phys. A: Math. Theor.*, vol. 45, p. 244035, 2012.

[29] P. Jaming and A. M. Powell, "Uncertainty Principles for Orthonormal Sequences," *J. Funct. Anal.*, vol. 243, no. 2, pp. 611–630, 2007.

[30] G. Matz, "Uncertainty and concentration inequalities for nonstationary random processes and time-frequency energy spectra," in *Proc. Asilomar Conf. Signals, Systems and Computers*, vol. 2, Nov. 2002, pp. 1571–1575 vol.2.

[31] G. de Abreu, "Closed-Form Correlation Functions of Generalized Hermite Wavelets," *IEEE Trans. Sig. Process.*, vol. 53, no. 6, pp. 2258–2261, 2005.

[32] N. G. de Bruijn, *Uncertainty Principles in Fourier Analysis*. New York: Academic Press, 1967, pp. 55–71.

APPENDIX A
PROOF OF THE BOUND ON THE GHP FOR ORTHOGONALLY MULTIPLEXED STOCHASTIC SIGNALS

For simplicity, we assume a signal which is centered at zero such that the overall mean in time and frequency is $\tilde{\mu}(x) = \tilde{\mu}(\hat{x}) = 0$. For any orthonormal sequence $\{\varphi_k\}_{k=0}^{N-1}$ in $L^2(\mathbb{R})$, where $N \geq 1$ and $\|\varphi_k\|_2 = 1 \,\forall\, k$, we have the following generalization of the Rayleigh quotient theorem to the Hilbert space [29]

$$\sum_k \langle O\,\varphi_k,\, \varphi_k\rangle \geq \sum_k \lambda_k(O), \tag{27}$$

where $\lambda_k(O)$ are the ordered eigenvalues of a positive self-adjoint operator O, such that $\lambda_0 < \lambda_1 < \cdots < \lambda_{N-1}$.

For functions φ in the Schwartz space[2] $\boldsymbol{S}(\mathbb{R}) \subset L^2(\mathbb{R})$, the Hermite operator H is defined by

$$H\,\varphi(t) = -\frac{1}{4\pi^2}\frac{d^2}{dt^2}\varphi(t) + t^2\varphi(t). \tag{28}$$

The Hermite-Gauss function $\varphi_k^{\mathrm{HG}} \in \boldsymbol{S}(\mathbb{R})$ is the eigenfunction of the above operator with eigenvalue $(2k+1)(2\pi)^{-1}$, such that

$$H\,\varphi_k^{\mathrm{HG}} = \frac{2k+1}{2\pi}\varphi_k^{\mathrm{HG}}. \tag{29}$$

For functions $\varphi \in L_2(\mathbb{R})$, Hermite operator H can be defined as a positive, self-adjoint, and unbounded operator, through the expansion $\varphi = \sum\langle\varphi, \varphi_k^{\mathrm{HG}}\rangle\varphi_k^{\mathrm{HG}}$ in the Hermite basis [29], [32]

$$H\,\varphi = \sum_{k=0}^{\infty}\frac{2k+1}{2\pi}\langle\varphi,\, \varphi_k^{\mathrm{HG}}\rangle\varphi_k^{\mathrm{HG}}, \tag{30}$$

from which it follows that

$$\langle H\varphi, \varphi\rangle = \sum_{k=0}^{\infty}\frac{2k+1}{2\pi}|\langle\varphi,\, \varphi_k^{\mathrm{HG}}\rangle|^2. \tag{31}$$

From (27) and the definition of the Hermite operator H follows the Mean-Dispersion Principle for orthonormal sequences, which states that [29]

$$\sum_k(\sigma_t^2(\varphi_k) + |\bar{t}(\varphi_k)|^2 + \sigma_f^2(\hat{\varphi_k}) + |\bar{f}(\hat{\varphi_k})^2|) \geq \sum_k \frac{2k+1}{2\pi}, \tag{32}$$

where $\bar{t}(\varphi_k)$ and $\bar{f}(\hat{\varphi_k})$ are the mean of φ_k in time and frequency, respectively. Because the sum of the variance and mean gives the second moment, the above inequality is equivalent to

$$\sum_k\int_{\mathbb{R}} t^2|\varphi_k(t)|^2dt + \sum_k\int_{\mathbb{R}} f^2|\hat{\varphi}_k(f)|^2df \geq \sum_k\frac{2k+1}{2\pi}, \tag{33}$$

from which we get

$$\tilde{\sigma}_t^2(x) + \tilde{\sigma}_f^2(\hat{x}) \geq \frac{N^2}{2\pi}. \tag{34}$$

To transform the sum of variances on the left of (34) to a product, and recover the form of the Heisenberg inequality, we perform the following optimization, as done in [32]. First, we define some constant $\alpha > 0$ and consider the functions

$$x'(t) = \alpha^{-1/2}x(t/\alpha)\ , \qquad \hat{x}'(f) = \alpha^{1/2}\hat{x}(f\alpha), \tag{35}$$

where $\hat{x}'(f)$ is the Fourier transform of $x'(t)$, such that $\hat{x}'(f) = \hat{x'}(f)$. By performing a change of variable in the

[2]The Schwartz space is the space of functions whose derivatives are rapidly decreasing [29].

involved integrals, we arrive at the following optimization problem

$$\alpha^2\tilde{\sigma}_t^2(x) + \alpha^{-2}\tilde{\sigma}_f^2(\hat{x}) \geq \frac{N^2}{2\pi}. \tag{36}$$

By minimizing the left with respect to α, we get the solution

$$\alpha = \tilde{\sigma}_t^{-1/2}(x)\tilde{\sigma}_f^{1/2}(\hat{x}), \tag{37}$$

which leads to the following Heisenberg-type inequality

$$\tilde{\sigma}_t(x)\tilde{\sigma}_f(\hat{x}) \geq \frac{N^2}{4\pi}. \tag{38}$$

Now, for the Heisenberg parameter generalized to the case where there are N component waveforms, we have

$$\tilde{\xi} = \frac{E[\|x\|_2^2]}{4\pi\tilde{\sigma}_t(x)\tilde{\sigma}_f(\hat{x})} \leq \frac{\sum_{k=0}^{N-1}\|\varphi_k\|_2^2}{4\pi\left(\frac{N^2}{4\pi}\right)} = \frac{1}{N}. \tag{39}$$

Appendix B
Proof of Proposition 1

Consider the Gabor system consisting of some $N = N_tN_f$ waveforms. Without loss of generality, let the N_t time translations and N_f frequency modulations of the prototype φ (with unit energy and duration T) be rectangular and symmetric around the origin, such that the lattice points are at multiples of T in $\mathcal{S} = \{-\frac{N_t-1}{2}, -\frac{N_t-1}{2}+1, \ldots, \frac{N_t-1}{2}-1, \frac{N_t-1}{2}\}$ in time, and are equivalently symmetric at multiples of $F = 1/T$ in frequency. The dispersion of stochastic signal x in time is given by

$$\tilde{\sigma}_t^2(x) = \sum_{k=0}^{N-1}\sigma_t^2(\varphi) + n_k^2T^2, \tag{40}$$

where we change variables for each k, and n_k is the coordinate of the kth component waveform with respect to the origin in time. Since there are N_f groups of N_t waveforms occupying the same frequency resources, we have

$$\tilde{\sigma}_t^2(x) = N\sigma_t^2(\varphi) + N_fT^2\sum_{m\in\mathcal{S}}m^2 \tag{41}$$

$$= N\left[\sigma_t^2(\varphi) + \frac{T^2}{12}(N_t^2-1)\right]. \tag{42}$$

By analogy, the frequency dispersion is given by

$$\tilde{\sigma}_f^2(x) = N\left[\sigma_f^2(\varphi) + \frac{F^2}{12}(N_f^2-1)\right]. \tag{43}$$

Finally, we have

$$\tilde{\xi}_{N_t,N_f,\mathrm{Gabor}}^2 = \frac{N^2}{16\pi^2\tilde{\sigma}_t^2(x)\tilde{\sigma}_f^2(\hat{x})}, \tag{44}$$

from which (17) with $a = 1$ follows directly.

In the case of OQAM on a staggered lattice, the real and complex waveforms are equivalent with respect to their variance, such that we may consider the entire lattice as two identical, half-power, N-component lattices separated by $T/2$ in the time domain. We then have the following for the overall time dispersion

$$\tilde{\sigma}_t^2(x) = \frac{1}{2}\sum_{k=0}^{N-1}\int_{\mathbb{R}}t^2\left|\varphi\left(t-(n_k\pm 1/4)\,T\right)\right|^2dt \tag{45}$$

$$= N\sigma_t^2(\varphi) + N_fT^2\sum_{m\in\mathcal{S}}(m+1/4)^2 \tag{46}$$

$$= N\left[\sigma_t^2(\varphi) + \frac{T^2}{12}(N_t^2-1/4)\right]. \tag{47}$$

The dispersion in the frequency domain remains the same as in (43). Then, from (44) follows (17) with $a = 1/4$.